Thermal spin fluctuation effect on the elastic constants of paramagnetic Fe from first principles

Zhihua Dong,[1,2,*] Wei Li,[1] Stephan Schönecker,[1,*] Song Lu,[1] Dengfu Chen,[2,*] and Levente Vitos[1,3,4]

[1]*Applied Materials Physics, Department of Materials Science and Engineering, Royal Institute of Technology, Stockholm SE-100 44, Sweden*

[2]*College of Materials Science and Engineering, Chongqing University, Chongqing 400030, People's Republic of China*

[3]*Department of Physics and Astronomy, Division of Materials Theory, Uppsala University, Box 516, SE-75121 Uppsala, Sweden*

[4]*Research Institute for Solid State Physics and Optics, Wigner Research Center for Physics, P.O. Box 49, H-1525 Budapest, Hungary*

(Received 14 September 2015; published 15 December 2015)

We investigate the impact of longitudinal thermal spin fluctuations on the temperature dependence of the elastic constants of paramagnetic body-centered-cubic (bcc) and face-centered-cubic (fcc) Fe. Based on a series of constrained local magnetic moment calculations, the spin fluctuation distribution is established using Boltzmann statistics and involving the Jacobian weight, and a temperature-dependent quadratic mean moment is introduced that accurately represents the spin fluctuation state as a function of temperature. We show that with increasing temperature, c' and c_{44} for the fcc phase and c_{44} for the bcc phase decrease at different rates due to different magnetoelastic coupling strengths. In contrast, c' in the bcc phase exhibits relatively high thermal stability. Longitudinal thermal spin fluctuations diminish the softening of both elastic constants in either phase and have comparatively large contributions in the fcc phase. In both bcc and fcc Fe, c_{44} has a larger temperature factor than c'. On the other hand, c' is more sensitive to the longitudinal thermal spin fluctuations, which balance the volume-induced softening by 21.6% in fcc Fe.

DOI: 10.1103/PhysRevB.92.224420 PACS number(s): 75.80.+q, 75.50.Bb, 71.15.Nc

I. INTRODUCTION

The great variety of thermodynamic and mechanical properties of Fe and its alloys are basically related to magnetism, which shows a high sensitivity to alloying and temperature. At ambient pressure, paramagnetic (PM) Fe is stable above 1043 K (Curie temperature), and it exhibits two transitions of the crystal structure from body-centered-cubic (bcc) to face-centered-cubic (fcc) phases at 1183 K and from fcc to bcc at 1667 K.

With increasing temperature, the excitations of atomic magnetic moments essentially brought by transversal and longitudinal spin fluctuations become an important question in itinerant-electron systems. In addition to the transversal fluctuations described by the Heisenberg model within the adiabatic approximation [1], a sizable contribution from longitudinal spin fluctuations to the Curie temperature of Fe, Co, and Ni and the relative stability of ferromagnetic hexagonal Co has been revealed by Uhl and Kübler using an improved Ginzburg-Landau-type Hamiltonian [2]. A similar relative importance of the longitudinal spin fluctuation was found by Sandratskii *et al.* [3,4] for ferromagnetic metals such as bcc Fe, fcc Ni, and even for half-metallic NiMnSb [5]. However, for PM Fe and Fe-based alloys stabilized at relatively high temperatures, and expectedly possessing large spin fluctuations, attempts to understand the role of spin fluctuation in their basic properties are still scarce. Among the limited number of works, the impact of spin fluctuation on cohesive [6,7] and elastic properties [8] of austenitic stainless steel at room temperature was discussed by means of the stacking fault energy, and by accounting for the local magnetic moment through contributions arising from magnetic entropy and phonon free energy. Longitudinal spin fluctuation distributions at certain temperatures were studied for PM bcc Fe and fcc Ni by Ruban *et al.* [9] using a magnetic Hamiltonian similar to that introduced by Shallcross *et al.* [10]. However, massive *ab initio* calculations are required to map out the parameters in this Hamiltonian formalism, making it less feasible to apply to complex systems such as multicomponent alloys.

Fundamental knowledge of elastic constants and their evolution with temperature contributes to the understanding of the great variety of intrinsic properties of Fe and its alloys, including the conspicuous magnetoelastic coupling. Despite the aforementioned efforts, an accurate prediction of the elastic properties of pure Fe at high temperatures remains elusive due to the complicated magnetic excitations and their interplay with the lattice expansion. In the present paper, the influence of thermal spin fluctuations on the elastic constants of both PM bcc and fcc Fe is introduced using a series of constrained disordered local magnetic moment calculations. Spin fluctuation distributions at various temperatures are described efficiently within the classical statistical thermodynamics via the Boltzmann distribution, and they are modeled as a multicomponent alloy described using the mean-field coherent-potential approximation [11,12]. To reduce the computational load, a mean local magnetic moment is introduced in a quadratic form, which is shown to accurately represent the spin fluctuation distribution as a function of temperature. Here we demonstrate the proposed methodology in the case of PM Fe. We show that the effect of longitudinal thermal spin fluctuations on the temperature factors of the two cubic shear elastic constants is not negligible compared to the changes driven merely by volume expansion. Due to its simplicity and efficiency, our methodology can easily be extended to multicomponent alloys containing several magnetic species. The extension will be evidenced in the case of Fe-Cr-Ni alloys in a further publication [13].

The rest of the paper is organized as follows. In Sec. II, we elaborate on the first-principles approach used in our calculations and the methodological details to establish both the spin fluctuation distributions and the mean local magnetic moment as a function of thermal excitations. The main results

*zhihuad@kth.se, stesch@kth.se, chendfu@cqu.edu.cn

are presented and discussed in Sec. III. The evolution of local magnetic moments and elastic constants with temperature considering the lattice expansion effect in combination with thermal spin fluctuations is presented and discussed for PM bcc and fcc Fe.

II. FIRST-PRINCIPLES CALCULATIONS

A. Total energy method

The self-consistent calculations were performed using density-functional theory (DFT) [14] in combination with the local-density approximation (LDA) [15], and the gradient terms were included in the total energy within the perturbative approach [16]. The Kohn-Sham equations were solved employing the exact muffin-tin orbitals (EMTO) method [17–20]. In this method, the effective potential is treated via the optimized overlapping muffin-tin approximation and the total energy is computed by using the full charge-density technique [18]. In the present application, the one-electron equations were solved within the scalar-relativistic approximation and the soft-core scheme.

The PM state of bcc and fcc Fe was described by the disordered local magnetic moment (DLM) approach [21] in combination with the coherent-potential approximation (CPA) [11,12]. Hence, all magnetic short-range-order effects were omitted, modeling at each temperature a completely random PM state.

The *ab initio* total energies were computed within the quasi-nonuniform gradient-level exchange-correlation approximation (QNA) introduced by Levämäki *et al.* [22,23]. The power and feasibility of this recently developed density-functional approximation to produce both highly accurate equilibrium volumes and bulk moduli of metals and alloys have been demonstrated in our previous work [23]. In the current paper, the QNA scheme designed for ferromagnetic bcc Fe was extended to PM bcc and fcc Fe. The present results demonstrate the transferability of the QNA from one magnetic and crystallographic system to another.

The theoretical equilibrium Wigner-Seitz radii (w) were determined from an exponential Morse-type function [24] fitted to the *ab initio* total energies. To calculate the two cubic shear moduli c' and c_{44}, we used volume-conserving orthorhombic and monoclinic deformations, respectively, as presented in Refs. [17,25]. The Brillouin zone sampling was done using uniformly distributed k points with density, which ensures the necessary numerical accuracy for elastic constant calculations.

B. Longitudinal thermal spin fluctuation model for the DLM state

At finite temperature (T), the magnitude of the disordered local magnetic moments (μ) fluctuates around the mean value. The continuous probability distribution for the magnitude of the random variable μ is replaced in our model by a distribution of discrete probabilities, $x_1^J, x_2^J, \ldots, x_n^J$. These probabilities involve the Jacobian weight μ_i^2 as originally introduced in Ref. [5], and they are discussed briefly below. At each temperature, we have $\sum_i x_i^J = 1$. Assuming single-site fluctuations, a PM state in the presence of longitudinal spin fluctuations may be modeled within a multicomponent DLM picture, viz.,

$$\mathrm{Fe}^{\uparrow\mu_1}_{x_1^J/2}\mathrm{Fe}^{\downarrow\mu_1}_{x_1^J/2}\cdots\mathrm{Fe}^{\uparrow\mu_i}_{x_i^J/2}\mathrm{Fe}^{\downarrow\mu_i}_{x_i^J/2}\cdots\mathrm{Fe}^{\uparrow\mu_n}_{x_n^J/2}\mathrm{Fe}^{\downarrow\mu_n}_{x_n^J/2} \tag{1}$$

with randomly distributed up ($\uparrow$) and down ($\downarrow$) local magnetic moments μ_i ($i = 1,2,\ldots,n$) on each alloy component. Thus, the probabilities x_i^J can be identified with the atomic fractions of the multicomponent random alloy in (1). The spin fluctuation distributions at each thermal excitation corresponding to temperature T are formulated using Boltzmann's factor,

$$x_i^J = \frac{1}{Z^J}\left(\frac{\mu_i}{\mu_\mathrm{B}}\right)^2 \exp\left[\frac{-E_i}{k_\mathrm{B}T}\right], \tag{2}$$

where $Z^J = \sum_{i=1}^n (\mu_i/\mu_\mathrm{B})^2 \exp\left[-E_i/k_\mathrm{B}T\right]$ is the partition function including the Jacobian weight μ_i^2, μ_B is the Bohr magneton, and k_B is the Boltzmann constant. Here E_i stands for the total energy of the single-impurity thermal spin fluctuation. That is, E_i represents the relative energy of the configuration where site i has the local magnetic moment μ_i embedded in a medium with mean magnetic moment $\langle\mu\rangle$. This energy is directly accessible from a series of multicomponent DLM calculations. In the present application, we approximate E_i by the energy of the binary $\mathrm{Fe}^{\uparrow\mu_i}_{0.5}\mathrm{Fe}^{\downarrow\mu_i}_{0.5}$ alloy with constrained magnetic moment μ_i, which is easily described by the regular constrained two-component DLM model. In the numerical calculations, an atomic moment scale ranging from 0 to $3.0\mu_\mathrm{B}$ with an interval of $0.5\mu_\mathrm{B}$ (i.e., $n = 7$) was adopted to map E_i. A convergence test for the partition of the probability distribution into n discrete values is presented in Sec. III B.

To reduce the computational load in studying the impact of thermal spin fluctuations on the bulk properties of complex multicomponent systems (not considered here), a mean magnetic moment, $m_\mathrm{sf}^J(\mu_i^2)$, is proposed in the quadratic form of the atomic moment as

$$m_\mathrm{sf}^J\left(\mu_i^2\right) = \sqrt{\sum_{i=1}^n \mu_i^2 x_i^J}. \tag{3}$$

By employing the mean moment from Eq. (3), the multicomponent spin fluctuation alloy model from (1) may be replaced by a binary alloy,

$$\mathrm{Fe}^{\uparrow m_\mathrm{sf}^J}_{0.5}\mathrm{Fe}^{\downarrow m_\mathrm{sf}^J}_{0.5}. \tag{4}$$

The physical picture behind the above approximation is that the energy depends approximately on the square of the local magnetic moment and thus the total energy obtained for the binary alloy (4) with local magnetic m_sf^J should be the best possible representation of the total energy calculated for the detailed distribution in (1). The accuracy of this approximation is established in Sec. III C by monitoring the predicted elastic constants of PM Fe at various temperatures using the original multicomponent scheme (1) and the binary one (4).

For comparison, we also consider the case when the Jacobian weight is excluded. The corresponding probabilities of spin density, x_i, and mean moment, $m_\mathrm{sf}(\mu_i^2)$, are

$$x_i = \frac{1}{Z}\exp\left[\frac{-E_i}{k_\mathrm{B}T}\right] \tag{5}$$

and

$$m_{\rm sf}(\mu_i^2) = \sqrt{\sum_{i=1}^{n} \mu_i^2 x_i}, \tag{6}$$

where the partition function without the Jacobian weight reads $Z = \sum_{i=1}^{n} \exp(-E_i/k_{\rm B}T)$. In addition to the quadratic mean moments from Eq. (3), we define an arithmetical mean moment

$$m_{sf}^{J}(\mu_i) = \sum_{i=1}^{n} \mu_i x_i^J. \tag{7}$$

The average moment applied in Ref. [5] corresponds to the arithmetical moments defined above.

Before closing this section, we briefly comment on the mean magnetic moments. Omitting the Jacobian weight corresponds to a model in which the longitudinal fluctuations of a moment are considered separately for each direction of the moment, and thus the statistical weight of the fluctuations does not depend on the size of the moment. It was found [5] that the actual size of the mean moments for NiMnSb and especially their temperature dependence depend sensitively on the Jacobian. Hence, we expect that the present mean moments $m_{\rm sf}^J$ and $m_{\rm sf}$ should also show different trends. On the other hand, the quadratic mean moment (3) used for the auxiliary binary system (4) should be a better approximation for the multicomponent spin fluctuation state (1) than the arithmetical mean moment (7), which is demonstrated below.

III. RESULTS AND DISCUSSION

A. Volume of PM Fe versus temperature

The theoretical volumes (represented here by the Wigner-Seitz radius $w_{\rm theor}$) at various temperatures were obtained by rescaling the calculated equilibrium Wigner-Seitz radius obtained for PM bcc and fcc Fe (corresponding to static conditions) using the experimental linear thermal expansion coefficient of 15.02 and 23.56×10^{-6} K^{-1} for PM bcc and fcc Fe, respectively [26]. The results are shown in Table I. Here we also list a few experimental values ($w_{\rm expt}$) that should be used to establish the accuracy of the present approach for the volume of PM Fe.

The theoretical volumes of bcc and fcc Fe are slightly lower than the experimental values, however the maximum of the absolute relative deviation is 0.43%. Such a good agreement between theory and experiment is not often seen, especially if one recalls the typical errors of common DFT schemes. The nearly perfect agreement in the present case is due to the QNA. The parameters of the QNA functional were obtained for ferromagnetic bcc Fe [22,23] and are extended here to PM bcc and PM fcc phases. The excellent performance of the QNA for these phases is a spectacular example showing the transferability of the QNA and that this scheme is flexible enough to produce highly accurate volumes even though both the magnetic state and the crystal structure of Fe vary.

TABLE I. Theoretical Wigner-Seitz radii $w_{\rm theor}$ for PM bcc and fcc Fe compared with the available experimental data $w_{\rm expt}$ from Ref. [26]. Temperature is in K, the Wigner-Seitz radius is in Bohr, and the relative deviation is in %.

System	T	$w_{\rm theor}$	$w_{\rm expt}$	Relative deviation
PM bcc	0	2.6513		
	1043	2.6928	2.6965	−0.14
	1120	2.6959	2.6993	−0.13
	1189	2.6986	2.7023	−0.14
PM fcc	0	2.6090		
	1189	2.6821	2.6931	−0.41
	1457	2.6986	2.7100	−0.42
	1661	2.7111	2.7228	−0.43

B. Local magnetic moments of PM Fe

The Boltzmann formula is a simple and elegant way to obtain the distribution of the longitudinal thermal spin fluctuation without performing time-consuming calculations of the parameters of a magnetic Hamiltonian. The input is the energy versus configuration, which is accessible from constrained DLM calculations. First we computed the total energy $\Delta E(\mu) = E^{\rm tot}(\mu) - E_0^{\rm tot}$ as a function of the DLM moment μ. Here $E_0^{\rm tot}$ represents the total energy of the nonmagnetic state. Then using this energy, we constructed the spin density distributions of PM bcc Fe at 1100 K and PM fcc Fe at 1400 K. For comparison, here we adopt both Eqs. (2) and (5). The results are presented in Fig. 1. These calculations were carried out at the corresponding theoretical Wigner-Seitz radius $w_{\rm bcc}(1100\ {\rm K}) = w_{\rm fcc}(1400\ {\rm K}) = 2.6951$ Bohr. The red and black transparent areas in the figure indicate the continuous distributions of spin density with (x_i^J) and without (x_i) involving the Jacobian weight, respectively. In the treatment of the three-dimensional fluctuations of atomic moments, for both PM bcc and fcc Fe, the Jacobian pushes the statistical weight to a larger magnitude of the local magnetic moment. In other words, spin fluctuations with large moment are more easily excited if the Jacobian weight is included, whereas fluctuations with small moment are more probable if the Jacobian weight is excluded. Compared to PM bcc Fe, a rather shallow minimum of the total energy curve is observed for PM fcc Fe, which makes excitation energetically more favorable and consequently produces a more uniform spin distribution, especially for the spin fluctuation in Eq. (5).

The mean magnetic moments calculated at constant volume are shown in Fig. 2 as a function of temperature between 1000 and 1500 K. Results from both spin densities including $[m_{\rm sf}^J(\mu_i^2)]$ and excluding $[m_{\rm sf}(\mu_i^2)]$ the Jacobian weight are presented for comparison. Excluding the Jacobian weight in the partition function, the mean magnetic moment $[m_{\rm sf}(\mu_i^2)]$ in PM bcc Fe declines smoothly from $1.960\mu_{\rm B}$ to $1.886\mu_{\rm B}$ with the temperature increasing from 1000 to 1500 K. The corresponding average decreasing rate of the local magnetic moment is around $1.5 \times 10^{-4}\mu_{\rm B}$ K^{-1}. The value is satisfyingly close to $1.4 \times 10^{-4}\mu_{\rm B}$ K^{-1} obtained at high temperature (between 1300 and 1500 K) using the magnetic Hamiltonian formalism [9]. For PM fcc Fe, the mean magnetic moment $m_{\rm sf}(\mu_i^2)$ decreases slightly from $1.554\mu_{\rm B}$ to $1.539\mu_{\rm B}$ in the same temperature range. Comparing the two crystallographic phases, the local magnetic moment in PM bcc Fe exhibits a slightly larger temperature slope than in PM fcc Fe.

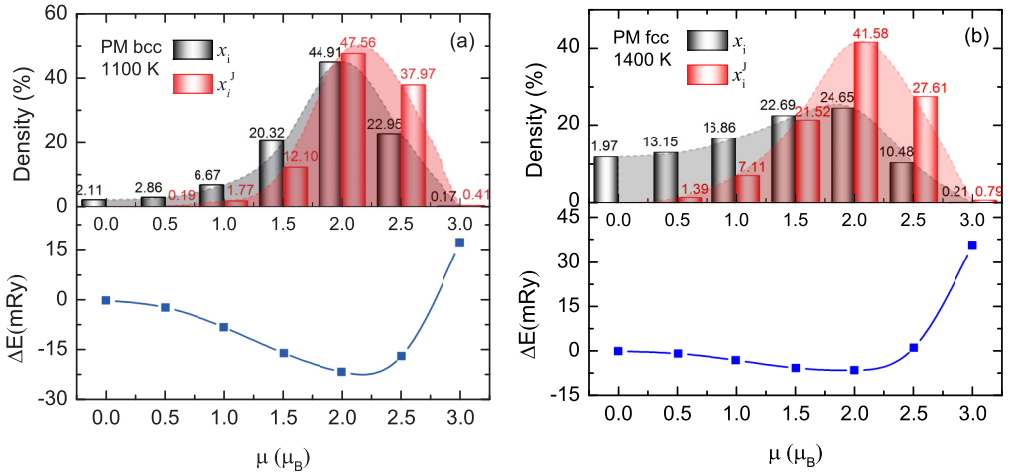

FIG. 1. (Color online) Total energy as a function of the local magnetic moment (lower panel) and the corresponding spin density distributions including and excluding the Jacobian weight (upper panel). Panel (a) is for PM bcc Fe at 1100 K and panel (b) is for PM fcc Fe at 1400 K. Calculations were performed for the theoretical Wigner-Seitz radii $w_{\rm bcc}(1100\ {\rm K}) = w_{\rm fcc}(1400\ {\rm K}) = 2.6951$ Bohr. The continuous spin density distributions are shown by the transparent areas.

When the Jacobian weight is included in the construction of the spin density distribution, the mean magnetic moment $m^J_{\rm sf}(\mu_i^2)$ becomes higher than $m_{\rm sf}(\mu_i^2)$ due to the large fraction of thermal excitations having large local moments (in Fig. 1). More importantly, the temperature dependences are reversed if the Jacobian weight is taken into account. Namely, the mean magnetic moment of PM bcc Fe shows a relatively weak temperature dependence, while that of PM fcc Fe clearly shows a positive slope with increasing temperature. As the temperature rises from 1000 to 1500 K, $m^J_{\rm sf}(\mu_i^2)$ increases linearly from $1.960\mu_{\rm B}$ to $2.015\mu_{\rm B}$ at a rate of $1.1 \times 10^{-4}\mu_{\rm B}\ {\rm K}^{-1}$ for PM fcc Fe, and it remains nearly constant ($2.112\mu_{\rm B}$–$2.120\mu_{\rm B}$) for PM bcc Fe.

The different temperature behaviors obtained with and without the Jacobian weight indicate two possible scenarios

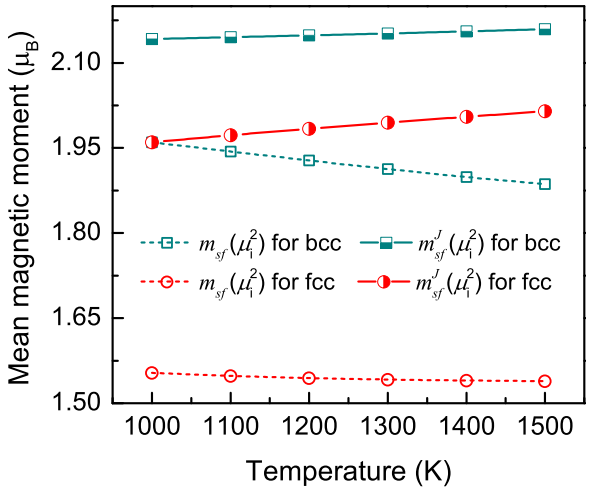

FIG. 2. (Color online) Mean local magnetic moments of PM bcc and fcc Fe from Eqs. (3) and (6) as functions of temperature. Both the mean magnetic moments with $[m^J_{\rm sf}(\mu_i^2)]$ and without $[m_{\rm sf}(\mu_i^2)]$ the Jacobian weight are presented. Calculations were performed for the theoretical Wigner-Seitz radii $w_{\rm bcc}(1100\ {\rm K}) = w_{\rm fcc}(1400\ {\rm K}) = 2.6951$ Bohr.

of thermal spin fluctuations. For the spin fluctuations treated separately for each direction, i.e., without the Jacobian weight, the probability of an atomic magnetic moment merely depends on the total energy of the configuration. In the spirit of Landau theory, we express the total energy as $\Delta E(\mu) \approx -a\mu^2 + b\mu^4 + c\mu^6 \ldots$, where a, b, and c are the usual Landau coefficients. For simplicity, we truncate the expansion after the sixth-order term (i.e., both a and c are positive). For the energies in Fig. 1, we find $a_{\rm bcc/fcc} \approx 8.2/2.6\ {\rm mRy}/\mu_{\rm B}^2$, $b_{\rm bcc/fcc} \approx 0.4/(-0.2)\ {\rm mRy}/\mu_{\rm B}^4$, and $c_{\rm bcc/fcc} \approx 0.1\ {\rm mRy}/\mu_{\rm B}^6$. Since the total energy is a strongly asymmetric function around the minimum, the atomic moments with small length are more likely to be excited with respect to the moments with large length. In PM fcc Fe, most of the atomic magnetic moments with small length are excited already at relatively low temperatures due to the very shallow minimum. This leads to a rather insensitive temperature dependence of the mean magnetic moment in the considered temperature interval (1000–1500 K). In PM bcc Fe, due to the deep total energy curve (notice $a_{\rm bcc} \gg a_{\rm fcc}$), the spin fluctuations are relatively difficult to excite at low temperatures. With increasing temperature, thermal spin fluctuations are continuously enhanced, especially in the low-moment range, and hence the mean bcc magnetic moment shows a negative temperature slope. On the other hand, including the Jacobian weight actually reflects the fact that the magnetic moments with large magnitude are preferably excited, i.e., the statistical weight is shifted toward larger μ values. This regime is dominated by the higher-order terms in the Landau expansion. Since $b_{\rm bcc} > b_{\rm fcc}$ and $c_{\rm bcc} \sim c_{\rm fcc}$, it is comparatively more difficult to induce large moments in the bcc phase as compared to the fcc phase. This explains the nearly vanishing thermal coefficient of $m^J_{\rm sf}(\mu_i^2)$ for bcc Fe as compared to the positive slope in the fcc phase (Fig. 1).

Before ending this section, we assess the influence of the spin fluctuation distributions corresponding to various n in Eqs. (3) and (6) on the mean moment and single-crystal elastic constants of PM Fe. The results of these tests are presented in Fig. 3 and listed in Table II. For simplicity, in these

TABLE II. Single-crystal elastic constants for two sets of magnetic moments involved in the spin fluctuation distribution without the Jacobian weight at 1100 and 1400 K for PM bcc and fcc Fe (corresponding to $w_{bcc}(1100\ K) = w_{fcc}(1400\ K) = 2.6951$ Bohr). The atomic moment range from 0 to $3.0\mu_B$ was used in both calculations ($n = 7$ and 16). The elastic constants are in GPa, temperature is in K, and the relative deviation is in %.

		interval $= 0.5\mu_B$ ($n = 7$)		interval $= 0.2\mu_B$ ($n = 16$)		Relative deviation	
System	T	c'	c_{44}	c'	c_{44}	c'	c_{44}
PM bcc	1100	7.99	111.25	8.14	111.23	1.86	−0.02
PM fcc	1400	40.57	127.46	39.67	126.57	−2.21	−0.70

additional calculations we used the spin density distribution excluding the Jacobian weight as in Eqs. (5) and (6). The calculations were carried out for the same magnetic moment region from 0 to $3.0\mu_B$ and employing different intervals corresponding to n values ranging from 7 to 120. Fitting an eighth-order Landau expression to the energies computed for $n = 7$, we also performed an analytical integration to get the "converged" mean moments, which are used for reference in Fig. 3 (dashed lines). We find that for small n values, the mean moments are slightly underestimated by Eq. (6) as compared to the values obtained by integration. However, the relative deviations are small. Namely, the maximum deviation in the mean moment at $n = 7$ is 0.37% and 2.94% for PM bcc and fcc Fe, respectively. We notice that when the Jacobian term is included, the convergence of the magnetic moment in terms of n is even better than the one shown in Fig. 3. In addition, very small variations in the elastic constants for both bcc and fcc Fe are obtained (Table II) as we go from $n = 7$ (modeled as a 14-component alloy) to $n = 16$ (modeled as a 32-component alloy). Based on these findings, we conclude that it is reasonable to use the initial scheme with the interval of $0.5\mu_B$ ($n = 7$) to study the effect of thermal spin fluctuation on the elastic constants.

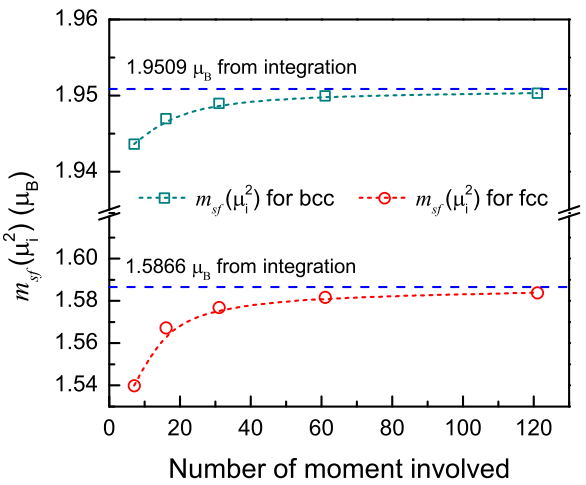

FIG. 3. (Color online) Mean local magnetic moment of PM bcc and fcc Fe from the spin density distributions excluding the Jacobian weight as a function of the number of distinct magnetic moments involved in the summation in Eq. (6). Calculations were performed for the atomic moment range from 0 to $3.0\mu_B$ using the theoretical Wigner-Seitz radius $w_{bcc}(1100\ K) = w_{fcc}(1400\ K) = 2.6951$ Bohr.

C. Elastic constants of PM Fe due to thermal spin fluctuation

The temperature dependence of the elastic parameters of PM stainless steel alloys was shown to have contributions from both volume expansion and spin fluctuation terms [8]. In the present work, first we computed the elastic constants of PM bcc and fcc Fe for a given constant volume by means of the spin fluctuation distribution and also by the average moment approximation. This test is expected to shed light on the impact of thermal spin fluctuation on the elastic constant of PM Fe (when excluding the volume effect), and also to establish the accuracy of our approach based on the mean moment in Eq. (3) used to represent the spin fluctuation distribution.

Results of the test performed for distributions including the Jacobian weights are presented in Table III. These calculations were performed at constant volume corresponding to $w_{bcc}(1100\ K) = w_{fcc}(1400\ K) = 2.6951$ Bohr. We find that for both fcc and bcc phases, c_{44} calculated using the arithmetic $[m^J_{sf}(\mu_i)]$ or the quadratic $[m^J_{sf}(\mu_i^2)]$ average in (4) are relatively close to that obtained from the spin fluctuation distribution, i.e., using x_i^J in (1). The relative deviations are below 0.53% for the bcc structure and 2.61% for the fcc structure. Somewhat larger deviations of c' computed with $m^J_{sf}(\mu_i)$ and $m^J_{sf}(\mu_i^2)$ are observed for both PM bcc and fcc Fe. However, the quadratic mean magnetic moment [Eq. (3)] turns out to have substantially higher accuracy than the arithmetical average [Eq. (7)]. The former leads to 0.68% and 2.36% relative deviations for the bcc and fcc phases, respectively, compared to 8.24% and 6.50% obtained for the latter.

TABLE III. Single-crystal elastic constant c' and c_{44} of PM Fe calculated for the spin fluctuation distribution including the Jacobian weight (x_i^J) and the mean moment from Eq. (7) [i.e., $m^J_{sf}(\mu_i)$] and the mean moment from Eq. (3) [i.e., $m^J_{sf}(\mu_i^2)$] for the same volume [corresponding to the theoretical Wigner-Seitz radii $w_{bcc}(1100\ K) = w_{fcc}(1400\ K) = 2.6951$ Bohr]. The relative deviations (RD) with respect to the predictions of the spin fluctuation distribution are presented in % and the elastic constants are in GPa.

System	Method	c'	RD of c'	c_{44}	RD of c_{44}
PM bcc (1100 K)	x_i^J	15.85		111.26	
	$m^J_{sf}(\mu_i)$	14.55	−8.24	110.67	−0.53
	$m^J_{sf}(\mu_i^2)$	15.75	−0.68	110.70	−0.50
PM fcc (1400 K)	x_i^J	24.00		114.70	
	$m^J_{sf}(\mu_i)$	25.56	6.50	112.85	−1.61
	$m^J_{sf}(\mu_i^2)$	23.44	−2.36	111.72	−2.61

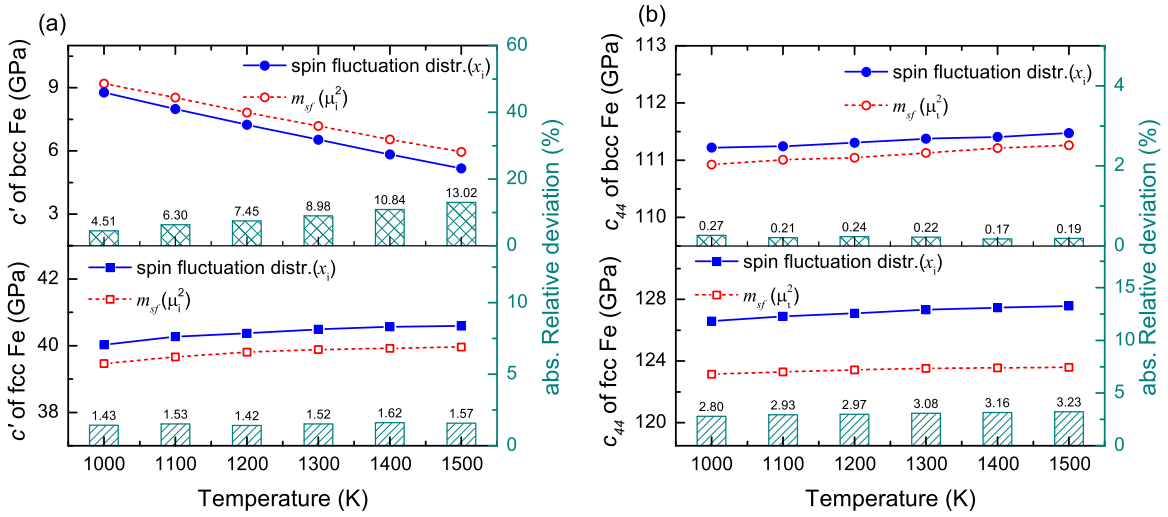

FIG. 4. (Color online) Single-crystal elastic constant c' (a) and c_{44} (b) of PM bcc Fe (upper panels) and PM fcc Fe (lower panels) calculated for the spin fluctuation distribution without the Jacobian weight and the mean moment [Eq. (6)] for the same volume [corresponding to the theoretical Wigner-Seitz radii $w_{\rm bcc}(1100\ {\rm K}) = w_{\rm fcc}(1400\ {\rm K}) = 2.6951$ Bohr] as a function of temperature. Absolute relative deviations between the results are shown by bars.

Similar assessments were carried out at various temperatures using the quadratic mean magnetic moment $[m_{\rm sf}(\mu_i^2)]$ with the spin density distribution excluding the Jacobian weight. As shown in Fig. 4, at constant volume, c' from the mean local magnetic moment is in good agreement with that from the spin fluctuation distribution for both bcc and fcc Fe. The absolute relative deviations (presented by bars) are below 1.62% for fcc and 13.02% for bcc phases. Although the maximum relative deviation of bcc Fe seems to be large, we should point out that the absolute deviation remains below 0.8 GPa for all temperatures considered here.

It is interesting to point out that while c' of bcc Fe decreases at a rate of $\sim 7.2 \times 10^{-3}$ GPa K^{-1} with increasing temperature, c' of fcc Fe indicates a weak increase ($\sim 1.1 \times 10^{-3}$ GPa K^{-1}) with temperature. Using the quadratic mean moment approach, nearly identical temperature factors of -6.5×10^{-3} and 1.0×10^{-3} GPa K^{-1} are obtained for bcc and fcc Fe, respectively. Similarly, c_{44} from the spin fluctuation distribution and the quadratic mean moment approach are consistent with each other, the largest relative deviation being less than 3.23%, as shown in Fig. 4(b). With increasing temperature, c_{44} of bcc and fcc Fe increases at a rate of $\sim 0.5 \times 10^{-3}$ and $\sim 2.0 \times 10^{-3}$ GPa K^{-1}, respectively.

Based on the above results, one may conclude that the mean magnetic moment approach introduced in Eq. (3) is a feasible representation of the spin fluctuation distribution. The obtained deviations between the two schemes are very small, which allows us to use the simplified scheme (binary alloy with mean local magnetic moment corresponding to the particular spin fluctuation distribution) to describe the impact of thermal spin fluctuation on the elastic parameters of PM bcc and fcc Fe.

Looking at the trends from Fig. 4, we observe that, for the spin fluctuations considered separately for each direction, except for c' of bcc Fe, the other single-crystal shear elastic parameters (c_{44} of PM bcc Fe and c' and c_{44} of PM fcc Fe) increase with temperature as a result of thermal longitudinal spin fluctuations (considered at fixed volume). These trends can be understood by combining the results for the thermal effect on the mean magnetic moment (see Sec. II B) with additional fixed-spin calculations, as illustrated below.

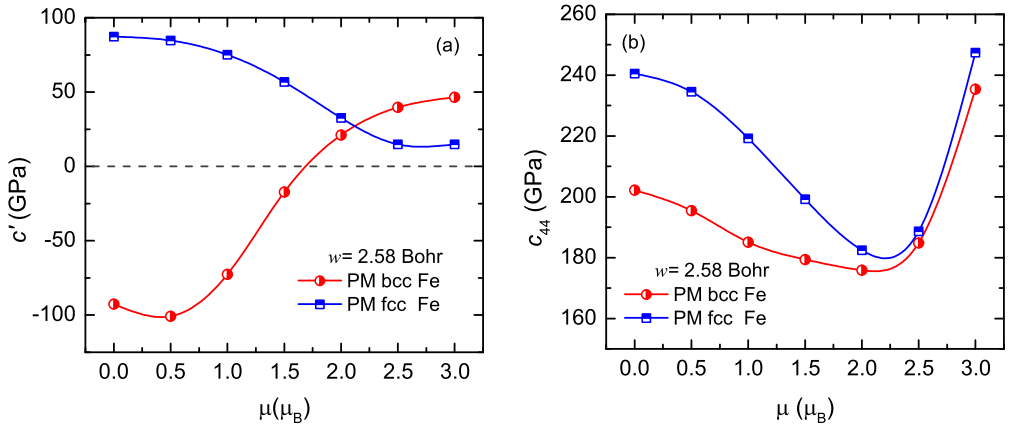

FIG. 5. (Color online) Single-crystal elastic constant c' (a) and c_{44} (b) of PM Fe as a function of the local magnetic moment on the Fe atoms. The fixed-spin calculations were performed with a constant Wigner-Seitz radius of 2.58 Bohr for both bcc and fcc Fe.

Fixed-spin DLM calculations for the local magnetic moment of PM Fe shown in Fig. 5(a) signal that smaller local magnetic moments favor larger c' in PM fcc Fe. This behavior is similar to that in PM Fe-Cr-Ni alloys [8]. However, c' of PM bcc Fe is found mostly to increase with increasing local magnetic moment, and the PM bcc phase is mechanically stable only at relatively large local magnetic moments. On the other hand, c_{44} of PM Fe initially declines with increasing local magnetic moment [in Fig. 5(b)], however the trend reverses when the local magnetic moment is beyond a critical value. c_{44} of PM Fe consequently indicates a minimum between $2.0\mu_B$ and $2.5\mu_B$. At fixed volume, the spin fluctuations considered separately for each direction decrease the magnitude of the mean magnetic moment as a function of temperature (Fig. 2). When combining these two effects, we obtain that spin fluctuations yield increasing (decreasing) c' for PM fcc (bcc) Fe and increasing c_{44} for PM Fe. These trends confirm nicely the results of the direct calculations shown in Fig. 4.

Based on this knowledge, we can also estimate the trends for the case when the Jacobian weight is included in the distribution. Combining the corresponding data in Fig. 2 with those in Fig. 5, we can infer that at constant volume when the spin fluctuations are treated in three dimensions, the temperature dependence of the elastic constants of PM Fe behaves in an opposite way. Namely, except for c' of bcc Fe, the other three single-crystal shear elastic parameters (c_{44} of PM bcc Fe and c' and c_{44} of PM fcc Fe) decrease with increasing temperature.

D. Temperature-dependent elastic constants of PM Fe

In the previous section, we investigated the impact of thermal spin fluctuations on the elastic parameters at fixed volume. To extend our study by taking into account additional important temperature factors, we attempt to account for the magnetovolume effect as well. Toward that end, first we formulated the spin fluctuation distributions including the Jacobian weight for various temperature-dependent volumes based on a series of *ab initio* DLM calculations. The underlying volume-temperature relationship is based on thermal expansion, as described in Sec. III A. Second, using the quadratic mean magnetic moments scheme in Eq. (3), the elastic constants of PM bcc and fcc Fe were computed as a function of temperature (employing the corresponding volume). We considered $T = 1000$, 1100, and 1200 K for bcc Fe and $T = 1200$, 1300, 1400, and 1600 K for fcc Fe. The present theoretical results are collected in Fig. 6, where we also show the available experimental data.

In Fig. 6, the theoretical and experimental Wigner-Seitz radii of the two PM phases are also shown. As already discussed in connection with the few data listed in Table I, the present theoretical Wigner-Seitz radii of PM Fe calculated using the QNA density-functional approximation are very close to the experimental values, especially for PM bcc Fe. The drop in volume at the crystal structure transition from bcc to fcc phase is obviously revealed. However, the volume collapse with increasing temperature is slightly overestimated by theory, which is due to the relatively large error found for fcc Fe. Upon the crystal structure change from bcc to fcc, c' and c_{44} increase by about 11 and 10 GPa, respectively,

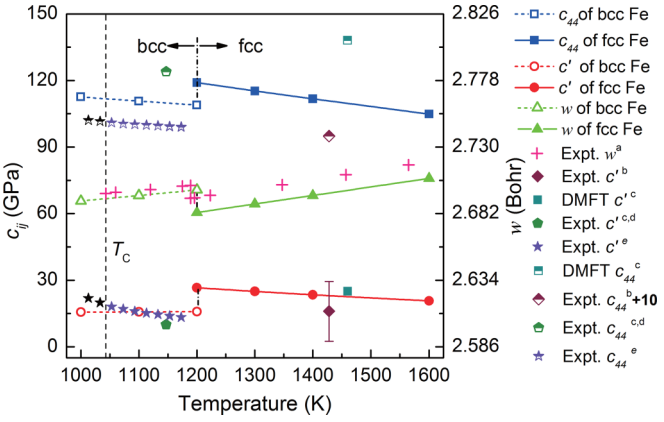

FIG. 6. (Color online) Single-crystal elastic constants, c' and c_{44}, and Wigner-Seitz radii of PM Fe as a function of temperature. The mean moments were calculated with Eq. (3) using the spin fluctuation distributions involving the Jacobian weight. The available experimental and former theoretical data are presented for comparison: [a]Ref. [26], [b]Ref. [28], [c]Ref. [29], [d]Ref. [30], and [e]Ref. [31]. The vertical dashed line denotes the Curie temperature ($T_C = 1043$ K) of Fe, and experimental results obtained below T_C in the ferromagnetic state are marked with black. The measured value for c_{44} from Ref. [28] is increased by 10 GPa, illustrated as "+10" in the figure to have a clear presentation. Some results in the figure are also listed (boldface) in Table IV for comparison.

indicating a strong structure dependence of the single-crystal elastic parameters. The jump in c' is in line with the total energy contour map of PM Fe [27]. Namely, since c' is connected with the curvature of the total energy as a function of tetragonal distortion (at constant volume), the smaller c' in the bcc phase compared to that of the fcc phase is an indication of the shallower energy minimum near the bcc phase within the Bain configurational space.

Compared to the limited experimental data and the former theoretical results obtained in the dynamical mean-field theory (DMFT) calculations [29], the present elastic constants show relative high accuracy for both PM bcc and fcc phases. Specifically, for the whole temperature range of the PM state, the predicted c' of PM bcc Fe are very close to the experimental measurements from Ref. [31], while the predicted c_{44} lie in the middle of the available experimental data. The temperature dependence of c_{44} is also correctly predicted as discussed in the following sections. For PM fcc Fe, in the present calculations c' is overestimated by around 7 GPa with respect to the experimental result from Ref. [28], however the theoretical prediction still falls within the limits of the error bar. Compared to the calculation from DMFT, c' is underestimated by $\sim$3 GPa in our predictions. Similarly, the c_{44} predicted here for PM fcc Fe lie between the experimental data and the DMFT value, indicating relatively high accuracy.

For comparison, the elastic constants of PM Fe were calculated using several alternative schemes. In particular, in addition to the spin fluctuation results [$m_{sf}^J(\mu_i^2)$], we performed floating spin calculations excluding (FS) and including (e-FS) electron excitations (Fermi distribution), constrained floating spin calculations without electron excitations (c-FS), and mean moment calculations based on the spin density distribution

TABLE IV. Single-crystal elastic constants of PM bcc and fcc Fe calculated using different schemes including floating spin excluding (FS) and including (*e*-FS) electron excitations, constrained floating spin without electron excitation (*c*-FS), the mean moment scheme from Eq. (3) based on the spin density distribution excluding the Jacobian weight [$m_{\rm sf}(\mu_i^2)$] and including the Jacobian weight [$m_{\rm sf}^J(\mu_i^2)$]. The elastic constants are in GPa, temperature is in K, and the Wigner-Seitz radius is in Bohr.

			$m_{\rm sf}(\mu_i^2)$		$m_{\rm sf}^J(\mu_i^2)$		FS		*c*-FS		*e*-FS	
System	T	w	c'	c_{44}	c'	c_{44}	c'	c_{44}	c'	c_{44}	c'	c_{44}
PM bcc	1000	2.6911	8.8	112.8	**15.6**	**112.6**	14.3	112.6	14.2	112.5		
	1100	2.6951	8.5	111.0	**15.7**	**110.7**	14.4	110.8	14.3	110.6		
	1200	2.6991	8.2	109.2	**15.8**	**108.9**	14.5	108.9	14.4	108.8	14.0	108.7
PM fcc	1200	2.6828	43.1	131.9	**26.6**	**119.1**	27.9	120.0	33.3	123.6		
	1400	2.6951	39.9	123.6	**23.4**	**111.7**	24.9	112.4	29.3	115.2		
	1600	2.7074	36.9	115.8	**20.7**	**104.9**	22.1	105.4	25.8	107.5	22.9	106.9

excluding the Jacobian weight [$m_{\rm sf}(\mu_i^2)$]. In the *c*-FS calculations, the atomic moment was fixed to the value from the self-consistent calculation without allowing for the magnetic relaxation upon lattice deformation. We notice that in spin fluctuation calculations, we always used a constrained scheme, i.e., the magnetic moment is conserved upon lattice distortion, and hence we speculate that comparing the FS and *c*-FS results could help us to estimate the size of the error associated with this constraint. The results of these additional calculations are collected in Table IV, and in the following we compare and discuss the various effects.

First, we consider the effect of electron excitations by comparing the results corresponding to the FS and *e*-FS schemes. The negligible influence of electron excitations on the elastic constants is signaled by the small deviations between the results for both bcc and fcc structures. Because of that, electron excitations were not included in the thermal spin fluctuation calculations in this work.

Second, we compare the FS results with those obtained in the *c*-FS scheme. The difference between the FS and *c*-FS results in Table IV shows how much the elastic constants change by keeping the magnetic moment fixed with lattice deformation compared to the case when the small deformation-induced magnetic relaxation is allowed. The differences are negligible for the bcc phase, but they are relatively large (∼3–5 GPa) for the fcc phase. Using this information, one can define a correction to the spin fluctuation results. Namely, we could eliminate the positive deviation in the elastic constants coming from the unrelaxed magnetic moment by decreasing c' and c_{44} of fcc Fe by ∼5 and ∼3 GPa, respectively (at relatively high temperatures). Notice that the so obtained "corrected" spin fluctuation values would come even closer to the reported experimental measurements.

Next, we consider the influence of thermal spin fluctuations by comparing the full results [$m_{\rm sf}^J(\mu_i^2)$] to those obtained in the *c*-FS scheme. It is found that thermal spin fluctuations favor larger c' in bcc Fe and smaller c' in fcc Fe than the corresponding *c*-FS data. Namely, thermal spin fluctuations lead to ∼1.4 GPa (∼ 9.0%) larger c' in bcc Fe and to ∼6.7 GPa (∼ 20.1%) smaller c' in fcc Fe as compared to the *c*-FS values. The opposite behavior for the two structures can be understood considering that thermal spin fluctuations give larger mean magnetic moments than the equilibrium (*c*-FS) moments (Figs. 1 and 2). Since c' increases (decreases) as the magnetic moment increases in the bcc (fcc) structure (Fig. 5), the above changes in the magnetic moments suggest larger (smaller) c' in bcc (fcc) upon allowing for thermal spin fluctuations. The c_{44} elastic parameter of fcc Fe decreases by ∼4.5 GPa due to thermal spin fluctuations, but little variation is observed in bcc Fe, which is due to the insensitive magnetoelastic coupling for c_{44} at relatively high local magnetic moments around $2.0\mu_{\rm B}$ for the bcc phase (Fig. 5).

Finally, we consider the effect of the Jacobian weight by comparing the results corresponding to $m_{\rm sf}(\mu_i^2)$ and $m_{\rm sf}^J(\mu_i^2)$. Omitting the Jacobian weight significantly decreases c' of bcc Fe (by ∼7.6 GPa) and increases c' of fcc Fe (by ∼16.5 GPa), yielding an even larger deviation relative to the experimental data. Thus, it seems to be a better treatment for the thermal spin fluctuation to include the Jacobian weight by considering the fluctuation in three dimensions rather than separately for each direction.

In the following section, we establish the temperature coefficients for the two cubic elastic constants for PM bcc and fcc Fe. As shown in Fig. 6, with increasing temperature, the theoretical c' increases in the bcc phase and decreases in the fcc phase at a rate of 0.116×10^{-2} and 1.469×10^{-2} GPa K^{-1}, respectively. Compared to the experimental measurements presented in Table V, the negative temperature dependence of c' for PM bcc Fe [$(2.3–5.5) \times 10^{-2}$ GPa K^{-1}] is not confirmed in the present thermal spin fluctuation calculations. We think

TABLE V. Theoretical volume expansion ($C_{\rm vol}$) and spin fluctuation ($C_{\rm spinf}$) contributions to the temperature dependence of the elastic constants (C) of PM bcc and fcc Fe. The temperature coefficients are expressed in units of 10^{-2} GPa K^{-1}. The total temperature dependence of the elastic constants ($C_{\rm tot}$) is also shown. The numbers in parentheses are the fractions (in %) contributed from the thermal spin fluctuations, i.e., $C_{\rm spinf}/C_{\rm vol}$ for c_{44} in bcc Fe, c' and c_{44} in fcc Fe, and $C_{\rm spinf}/C_{\rm tot}$ for c' in bcc Fe. For comparison, the available experimental coefficient ($C_{\rm expt}$) in Ref. [31] for iron and Ref. [33] for steel Fe15Cr15Ni are also included.

System	C	$C_{\rm vol}$	$C_{\rm spinf}$	$C_{\rm tot}$	$C_{\rm expt}$
PM bcc	c'	0.103	0.013 (11.3)	0.116	$-2.3\sim-5.5$
	c_{44}	−1.850	0.030 (−1.6)	−1.820	−1.6
PM fcc	c'	−1.874	0.405 (−21.6)	−1.469	−2.1[a]
	c_{44}	−4.019	0.490 (−12.2)	−3.529	−4.9[a]

[a]The temperature coefficients are derived at room temperature for the Fe15Cr15Ni alloy.

that the actual physical mechanism behind the increasing temperature coefficient as the temperature approaches the Curie temperature (T_C) from above is the enhancement of the magnetic short-range order. Namely, with decreasing temperature in the PM state, the magnetic ordering in the bcc phase gradually increases and transforms to a completely ordered ferromagnetic state below T_C. The decisive role of the magnetic short-range order in stabilizing the bcc phase above the magnetic transition temperature has indeed been demonstrated by recent DMFT [29] and DFT [32] calculations. The temperature coefficient consequently increases with the magnetic ordering and produces a relatively high-temperature coefficient of 8.6×10^{-2} GPa K^{-1} in ferromagnetic bcc Fe as shown in Fig. 6. During the thermal spin fluctuation calculations, a completely random PM state was assumed by adopting the DLM picture. We suggest that omitting the effect of magnetic short-range order close to T_C is the reason for the different temperature slope in the present theory as compared to the observations. In the fcc structure, despite the deviations due to the thermal and alloying effects, the predicted temperature coefficient of c' indicates a better agreement with the experimental result for steel Fe15Cr15Ni (2.1×10^{-2} GPa K^{-1}) than that in the bcc structure. For c_{44} of PM Fe, the theoretical predictions for the bcc and fcc phases decrease linearly at a rate of 1.820×10^{-2} and 3.529×10^{-2} GPa K^{-1}, respectively. The temperature coefficient of c_{44} for PM bcc Fe shows good agreement with 1.6×10^{-2} GPa K^{-1} from experiment, and the influence of magnetic ordering near T_C on this temperature coefficient seems to be less pronounced. In the fcc phase, the theoretical temperature coefficient of c_{44} is also comparable to the experimental data of steel Fe15Cr15Ni presented in Table V.

To understand the temperature coefficient $C \equiv \Delta c/\Delta T$ of the elastic constant c of PM Fe and its dependence on thermal spin fluctuations, the contributions from volume expansion and spin fluctuation are quantitatively estimated. These results are presented in Table V. The contribution from the volume expansion is built up from the c-FS calculations to eliminate the effect of constrained atomic moment during deformation. Then the spin fluctuation contribution to the temperature coefficient is conveniently extracted from the difference between the full results [$m_{sf}^J(\mu_i^2)$] and the c-FS results, i.e., $C_{spinf} = C_{tot} - C_{vol}$. Here C_{tot} is the total temperature coefficient of the elastic constants, C_{spinf} and C_{vol} represent the partial temperature factors arising from the thermal spin fluctuation and the volume expansion, respectively.

From the temperature factors presented in Table V, we infer that C_{spinf} is positive, diminishing the softening of both elastic constants as the temperature increases in fcc and bcc phases. Furthermore, they show a comparatively large contribution in fcc structure, indicating consistency with the trends shown in Fig. 2. In fcc Fe, the relatively high decreasing rate of c' is primarily related to the volume-induced softening, whereas thermal spin fluctuations balance by 21.6% approximately. The weak increase of c' for bcc Fe is determined by the positive contribution from the volume expansion. Compared to c', c_{44} shows relatively larger temperature factors for both PM bcc and fcc Fe, however the thermal spin fluctuations give smaller relative contributions. In bcc Fe, almost the whole decrease in c_{44} is due to the volume softening, which completely screens the small positive effect from the spin fluctuations. However, the contribution from spin fluctuation is increased to around 12.2% in fcc Fe.

IV. CONCLUSIONS

Using the exact muffin-tin orbital method in combination with the coherent-potential approximation and the disordered local moment scheme, we have investigated the effect of thermal spin fluctuations on the local magnetic moments and elastic parameters of PM bcc and fcc Fe. The spin fluctuation distribution was formulated using the Boltzmann factor including the Jacobian weight. The mean local magnetic moment in quadratic form has been demonstrated to be a feasible representation of the spin fluctuation distribution. Coupling the spin fluctuation and the volume expansion effects, the temperature dependence of the mean local magnetic moments and elastic constants of PM bcc and fcc Fe have been discussed. The elastic constants of PM Fe except for c' of the bcc phase decrease with increasing temperature, and c_{44} shows a faster decreasing rate. In both bcc and fcc Fe, the spin fluctuations diminish the decreasing process and have a relatively large contribution in fcc Fe. Compared to c_{44}, thermal spin fluctuations have a stronger relative effect on the temperature dependence of c' in PM Fe. The presently introduced calculational scheme is based on thermodynamics in combination with alloy theory, and it offers a simple and transparent route that can easily be extended to more complicated cases such as multicomponent PM steel alloys or high-entropy alloys.

ACKNOWLEDGMENTS

Work was supported by the Swedish Research Council, the Swedish Foundation for Strategic Research, the Chinese Scholarship Council, and the Hungarian Scientific Research Fund (OTKA 84078 and 109570). The National Natural Science Foundation of China (NSFC, Project No. 51374260), the Natural Science Foundation of Chongqing (Project No. cstc2013jcyjA50005), and the State Key Laboratory of Advanced Metallurgy of China (Project No. KF13-01) are also acknowledged.

[1] B. L. Györffy, A. J. Pindor, J. Staunton, G. M. Stocks, and H. Winter, J. Phys. F **15**, 1337 (1985).
[2] M. Uhl and J. Kübler, Phys. Rev. Lett. **77**, 334 (1996).
[3] L. M. Sandratskii and E. N. Kuvaldin, J. Phys. Condens. Matter **3**, 7663 (1991).
[4] F. Dietermann, L. M. Sandratskii, and M. Fähnle, J. Magn. Magn. Mater. **324**, 2693 (2012).
[5] L. M. Sandratskii, Phys. Rev. B **78**, 094425 (2008).
[6] L. Vitos, P. A. Korzhavyi, and B. Johansson, Phys. Rev. Lett. **96**, 117210 (2006).
[7] L. Vitos, J. O. Nilsson, and B. Johansson, Acta Mater. **54**, 3821 (2006).
[8] L. Vitos and B. Johansson, Phys. Rev. B **79**, 024415 (2009).

[9] A. V. Ruban, S. Khmelevskyi, P. Mohn, and B. Johansson, Phys. Rev. B **75**, 054402 (2007).
[10] S. Shallcross, A. E. Kissavos, V. Meded, and A. V. Ruban, Phys. Rev. B **72**, 104437 (2005).
[11] P. Soven, Phys. Rev. **156**, 809 (1967).
[12] B. L. Györffy, Phys. Rev. B **5**, 2382 (1972).
[13] Z. H. Dong and L. Vitos (unpublished).
[14] P. Hohenberg and W. Kohn, Phys. Rev. **136**, B864 (1964).
[15] W. Kohn and L. J. Sham, Phys. Rev. **140**, A1133 (1965).
[16] M. Asato, A. Settels, T. Hoshino, T. Asada, S. Blügel, R. Zeller, and P. H. Dederichs, Phys. Rev. B **60**, 5202 (1999).
[17] L. Vitos, *Computational Quantum Mechanics for Materials Engineers: The EMTO Method and Applications, Engineering Materials and Processes Series* (Springer London, 2007), p. 235.
[18] L. Vitos, I. A. Abrikosov, and B. Johansson, Phys. Rev. Lett. **87**, 156401 (2001).
[19] L. Vitos, H. L. Skriver, B. Johansson, and J. Kollár, Comput. Mater. Sci. **18**, 24 (2000).
[20] J. Kollár, L. Vitos, and H. L. Skriver, in *Electronic Structure and Physical Properties of Solids: The Uses of the LMTO Method*, edited by H. Dreysse (Springer-Verlag, Berlin, 2000), p. 85.
[21] J. Staunton, B. L. Györffy, A. J. Pindor, G. M. Stocks, and H. Winter, J. Magn. Magn. Mater. **45**, 15 (1984).
[22] H. Levämäki, M. P. J. Punkkinen, K. Kokko, and L. Vitos, Phys. Rev. B **86**, 201104 (2012).
[23] H. Levämäki, M. P. J. Punkkinen, K. Kokko, and L. Vitos, Phys. Rev. B **89**, 115107 (2014).
[24] V. L. Moruzzi, J. F. Janak, and K. Schwarz, Phys. Rev. B **37**, 790 (1988).
[25] A. Taga, L. Vitos, B. Johansson, and G. Grimvall, Phys. Rev. B **71**, 014201 (2005).
[26] Z. S. Basinski, W. Hume-Rothery, and A. L. Sutton, Proc. R. Soc. A **229**, 459 (1955).
[27] H. L. Zhang, N. Al-Zoubi, B. Johansson, and L. Vitos, J. Appl. Phys. **110**, 073707 (2011).
[28] J. Zarestky and C. Stassis, Phys. Rev. B **35**, 4500 (1987).
[29] I. Leonov, A. I. Poteryaev, V. I. Anisimov, and D. Vollhardt, Phys. Rev. B **85**, 020401 (2012).
[30] J. Neuhaus, W. Petry, and A. Krimmel, Physica B **234-236**, 897 (1997).
[31] D. J. Dever, J. Appl. Phys. **43**, 3293 (1972).
[32] H. Zhang, B. Johansson, and L. Vitos, Phys. Rev. B **84**, 140411 (2011).
[33] A. Teklu, H. Ledbetter, S. Kim, L. A. Boatner, M. McGuire, and V. Keppens, Metall. Mater. Trans. A **35**, 3149 (2004).